HHS Public Access

Author manuscript

Nat Med. Author manuscript; available in PMC 2015 August 01.

Published in final edited form as:

Nat Med. 2015 February ; 21(2): 192–197. doi:10.1038/nm.3728.

Structure-Inherent Targeting of NIR Fluorophores for Parathyroid and Thyroid Gland Imaging

Hoon Hyun[1,*], **Min Ho Park**[1,2,*], **Eric A. Owens**[3], **Hideyuki Wada**[1], **Maged Henary**[3], **Hein J.M. Handgraaf**[5], **Alexander L. Vahrmeijer**[5], **John V. Frangioni**[1,4,6], and **Hak Soo Choi**[1,7,**]

[1]Division of Hematology/Oncology, Department of Medicine, Beth Israel Deaconess Medical Center and Harvard Medical School, Boston, MA 02215 [2]Department of Surgery, Chonnam National University Medical School, Gwangju 501-746, South Korea [3]Department of Chemistry, Georgia State University, Atlanta, GA 30303 [4]Department of Radiology, Beth Israel Deaconess Medical Center and Harvard Medical School, Boston, MA 02215 [5]Department of Surgery, Leiden University Medical Center, Leiden, the Netherlands [6]Curadel, LLC, 377 Plantation Street, Worcester, MA 01605 [7]Department of Cogno-Mechatronics Engineering, Pusan National University, Busan 609-735, South Korea

Abstract

The typical method for creating targeted contrast agents requires covalent conjugation of separate targeting and fluorophore domains. In this study, we demonstrate that it is possible create tissue-specific near-infrared fluorophores using the inherent chemical structure. Thus, a single compact molecule performs both targeting and imaging. We use this strategy to solve a major problem in head/neck surgery, the identification and preservation of parathyroid and thyroid glands. We synthesized 700-nm and 800-nm halogenated fluorophores that show high uptake in the specific glands after a single intravenous injection of only 0.06 mg kg^{-1} in a pig. Using a dual-channel near-infrared imaging system, we demonstrate the real-time, high-sensitivity, unambiguous identification of parathyroid and thyroid glands simultaneously in the context of blood and surrounding soft tissue. This novel technology lays the foundation for head/neck surgery performed with increased precision and efficiency, and potentially lowers morbidity, and a general strategy for targeted near-infrared fluorophore development.

Corresponding Author: Hak Soo Choi, Ph.D., 330 Brookline Avenue, Room SL-436A, Boston, MA 02215, Office: 617-667-6024; Fax: 617-975-5016, hchoi@bidmc.harvard.edu.

*These authors contributed equally to this work.

AUTHOR CONTRIBUTIONS

HH, MHP, HW, EAO, and HJMH performed the experiments. HH, MHP, MH, ALV, JVF, and HSC reviewed, analyzed, and interpreted the data. HH, JVF, and HSC wrote the paper. All authors discussed the results and commented on the manuscript.

COMPETING FINANCIAL INTERESTS

John V. Frangioni, M.D., Ph.D.: Dr. Frangioni is currently CEO of Curadel, LLC, which has licensed FLARE imaging systems and contrast agents from the Beth Israel Deaconess Medical Center.

Keywords

Near-infrared fluorescence; targeted fluorophore; optical imaging; image-guided surgery; signal-to-background ratio

INTRODUCTION

A fundamental problem in image-guided surgery is the development of contrast agents that are targeted to specific normal or diseased tissues[1–5]. Recently, near-infrared (NIR) fluorophores have become the imaging technology of choice because of relatively low photon tissue attenuation, low autofluorescence, and target detection depths up to 5 mm (reviewed in [6]). Almost all targeted NIR fluorophores described to date require covalent conjugation of a targeting domain (i.e., small molecule, peptidomimetic, peptide, antibody, etc.) to an NIR fluorophore. Although this strategy can work well, NIR fluorophores are relatively large molecules (500–1200 Da) to begin with, and chemical synthesis of conjugates can sometimes be time-consuming. An alternative, albeit difficult, approach is to create NIR fluorophores whose inherent chemical structure provides specific targeting to a tissue of interest.

The endocrine glands are tissues of significant clinical importance, yet are difficult to find during surgery[7]. In particular, partial or complete resection of the thyroid gland requires accurate identification and preservation of the parathyroid glands. Complications can occur when all functional parathyroid glands are inadvertently damaged or removed during thyroidectomies, or are incompletely removed during parathyroidectomies[8,9]. Damage to these tiny organs can have deleterious, life-long effects on patient health because they secrete hormones responsible for the regulation of blood calcium levels, and hypocalcemia can ensue.

The identification of normal parathyroid glands and accessory thyroid tissue with the naked eye is still challenging in high risk procedures, such as re-operative central neck surgery, thyroid cancer, and Graves' disease[9,10]. Not only are they small, but their location also varies widely from person to person and it takes microscopy to reliably tell the difference between parathyroid tissue, thyroid tissue, and lymph nodes that surround them[10]. Existing methods for identifying parathyroid glands rely on histopathology or postoperative evaluation to determine if they were accidentally or incompletely removed. However, surgical biopsy of the parathyroid for identification can lead to devascularization and destruction of their function. Consequently, surgeons must now rely on visual inspection to identify the different tissues, which can be subjective and inconclusive[11].

The goal of this study was to create families of halogenated 700 nm and 800 nm NIR fluorophores that exhibited specific uptake in parathyroid glands, thyroid glands, or both by virtue of their inherent chemical structure. Such molecules could provide surgeons with unambiguous guidance during head and neck surgery after a simple intravenous injection.

RESULTS

Synthesis and characterization of T700 and T800 fluorophores

An initial screen of a NIR fluorophore library containing 280 novel compounds injected intravenously into CD-1 mice identified two potential pharmacophore for thyroid uptake, one for 700 nm emission and the other for 800 nm emission (data not shown). We then prepared a series of new compounds built around these pharmacophores to optimize endocrine gland uptake. The synthetic methods for the preparation of T700 (compounds **13**−**17**) and T800 (compounds **18**−**22**) are shown in Figure 1a and Supplementary Methods. T700 and T800 NIR fluorophores, emitting at 700 nm and 800 nm, respectively, were composed of pentamethine or heptamethine cores decorated with various side chains, including H, OMe, F, Cl and Br. Prior to measurement of optical properties and *in vivo* performance, each NIR fluorophore was purified to ≥ 95% as measured using 210 nm absorbance (Supplementary Fig. S1).

Physicochemical and optical properties of T700 and T800 NIR fluorophores are summarized in Figure 1b. By varying the side chains of the polymethine core, it was possible to systematically modify hydrophilicity, hydrophobicity, polarity, and electron resonance. All targeted NIR fluorophores exhibited maximum fluorescence in the range of 650 to 780 nm wavelength and high extinction coefficients and quantum yields, which together minimize tissue autofluorescence and maximize fluorescence signal (Supplementary Fig. S2).

Autofluorescence of thyroid and parathyroid glands

Before testing targeted compounds in thyroid and parathyroid glands, autofluorescence of both glands were imaged in human and pig (Supplementary Fig. S3). For human study, subjects undergoing neck dissection as part of a separate ongoing study were imaged consecutively with Channel #1 (700 nm NIR) and Channel #2 (800 nm NIR) of the mini-FLARE imaging system after exposure and/or resection of normal parathryoid and thyroid glands. There is no significant autofluorescence above background in the parathyroid glands in human and pig. However, faint autofluorescence of thyroid gland was observed after a long exposure time (250 msec) at 700 nm.

In vivo thyroid imaging of T700 and T800 in mice

As a preliminary *in vivo* test for thyroid targeting, T700 and T800 NIR fluorophores were intravenously injected into CD-1 mice (10 nmol; 0.2 mg kg^{-1}), imaged after 1 h and 4 h, and the thyroid signal quantified (Fig. 2). T700-F and T800-F showed the highest signal-to-background ratio (SBR, calculated by fluorescence intensities between thyroid and neighboring muscle) values compared to the other molecules. Signal intensity decreased only 17% between 1 and 4 h post-injection. Salivary gland uptake, which is common in rodents, is a non-issue in humans because of their submandibular location.

Because T700-F and T800-F showed the highest SBR for thyroid among the different side chains, we selected these F-appended NIR fluorophores for further *in vivo* study. To determine the optimal dose of T700-F and T800-F for thyroid imaging, 10 to 100 nmol (0.2 – 2.0 mg kg^{-1}) was injected intravenously into mice and the SBR measured over time. As

shown in Supplementary Figure S4, a dose of 50 nmol (1.0 mg kg^{-1}) was optimal for single intravenous injection for a CD-1 mouse. With respect to clearance and elimination, T700-F exhibited primarily renal clearance and T800-F accumulated in both liver and kidneys 4 h post-injection (Supplementary Fig. S5). However, the fluorescent absolute amounts of fluorophore excreted into urine and feces were low and difficult to detect at 4 h post-injection.

In vivo parathyroid and thyroid imaging in pigs

We employed pigs as a large animal model for parathyroid identification because they represent a worst-case scenario. Unlike humans, pig parathyroid glands are located in the thorax, far from the thyroid glands, and without anatomical landmarks.[12] T700-F and T800-F were intravenously injected into separate Yorkshire pigs at a dose of 5 μmol (0.06 mg kg^{-1}) and imaged over a period of 5 h (Fig. 3). Both T700-F and T800-F identified pig parathyroid with high sensitivity and specify. We believe that this is the first demonstration of pig parathyroid imaging *in vivo*. It should be noted how difficult it is to distinguish pig parathyroid glands with the naked eye because of their small size (a few millimeters) and embedding within surrounding thymus. Interestingly, T800-F showed higher fluorescence in parathyroid 1 h post-injection, and signal was maintained for over 5 h, while T700-F showed lower parathyroid fluorescence compared to thyroid fluorescence and parathyroid signal decreased significantly over time. The parathyroid to thyroid signal ratio (PTR) curves indicate that T800-F can be used for identification of parathyroid glands even when T700-F shows equal signal in thyroid and parathyroid glands.

Simultaneous *in vivo* NIR imaging of parathyroid and thyroid

To provide surgeons with unambiguous landmarks during head and neck sugary, we exploited the dual-NIR channel capability of the FLARE imaging system to highlight parathyroid and thyroid glands simultaneously and in real time. For initial experiments we chose rats because they possess a single pair of parathyroid glands located on the anterior and lateral aspect of the thyroid lobes[13]. For dual-channel imaging of parathyroid and thyroid glands, 0.2 μmol (0.35 mg kg^{-1} of T800-F was intravenously injected into a 250 g SD rat 24 h prior to imaging, followed by 0.2 μmol of T700-F injected into the same animal 6 h prior to imaging. The doses and timing used are the optimal ones found during initial screening tests in rats (data not shown). Under these conditions, T800-F visualizes parathyroid glands unambiguously, whereas T700-F simultaneously highlights thyroid glands (Fig. 4a). The identities of resected tissues were confirmed using NIR fluorescence microscopy and consecutive H&E staining (Fig. 4b). As expected, T700-F was seen staining both thyroid and parathyroid glands, while T800-F remained only in parathyroid gland.

To confirm that these results were species-independent, experiments were repeated in pig using 5 μmol (0.06 mg kg^{-1}) of T800-F injected intravenously followed 2 h later by 5 μmol of T700-F. As presented in Figure 5, T700-F targeted both follicular and parafollicular cells of pig thyroid, while T800-F targeted the chief cells and oxyphil cells of pig parathyroid.

DISCUSSION

By incorporating tissue targeting into the chemical structure of a fluorophore, one creates the most compact possible bifunctional contrast agent. This strategy eliminates the need for covalent conjugation of targeting and fluorophore domains and facilitates subsequent optimization of other *in vivo* properties, such as biodistribution, clearance, and elimination. Of course, finding such contrast agents is a laborious task, which in our case required synthesis and screening of a relatively large NIR fluorophore library (≥ 280) then optimizing the presumed pharmacophore. Nevertheless, the strategy is applicable to virtually any desired target and as the NIR fluorophore library increases in size, pharmacophores for any particular target become more robust[14,15].

The only other agent known to target glands in the head and neck is methylene blue[16,17], which displays uptake in a tumor of the parathyroid called a parathyroid adenoma but not normal parathyroid glands. Moreover, methylene blue has a completely different chemical structure (phenothiazine derivative) from T700-F (pentamethine cyanine) and T800-F (heptamethine cyanine) as well as relatively poor optical properties, especially compared to T800-F.

Two recent studies by Mahadevan-Jansen and colleagues[18,19] suggest that human parathyroid and thyroid has detectable autofluorescence. This may be true at fluence rates over 5000-fold higher than those used in our study, or as a result of the local diet of study subjects, however, we have not found significant autofluorescence in either of these glands in 5 species studied to date, including humans. Moreover, the need to identify and resect the glands prior to contact probe-based spectroscopy negates the utility of real-time image guidance.

Judicious choice is required when matching contrast agents to specific procedures. Based on first principles, 800 nm NIR light provides SBRs of 2- to 10-fold higher than 700 nm light due to the combined effects of absorption, scatter, extinction coefficient, and autofluorescence[20]. This is true even though silicon CCDs have a lower quantum efficiency at 800 nm versus 700 nm. Thus, we always employ 800 nm emitting NIR fluorophores and Channel #2 of the FLARE imaging system when working with small targets (e.g., parathyroid glands), dim targets, or targets embedded deep in tissue. Conversely, 700 nm emitting NIR fluorohores and Channel #1 are typically employed for large targets (e.g., thyroid) or bright targets. Having two independent NIR fluorescence channels permits complex surgeries to be performed under complete image-guidance. Take, for example, Graves' disease, where the surgeon has two simultaneous tasks, namely to find all thyroid tissue including accessory thyroid tissue in the neck, as well as to idendify, resect without damage, and reimplant funcitonal parathryoid glands. The combination of contrast agents and imaging system described in our study now makes real-time guidance throughout this complex procedure possible.

The mechanism of uptake and retention of T700-F and T800-F in specific cell types of the thyroid and parathyroid glands is presently unknown. However, it appears that site-specific halogenation of the polymethine core is critical for targeting, and it is possible that cellular

machinery (transporters, enzymes, etc.) that process iodine may be mistaking these molecules as endogenous substrates. Future studies could be directed at identification of the intracellular targets of these contrast agents, although it should be noted that contrast agent optimization can continue knowing only the target cell type and preliminary pharmacophore.

In summary, the ability to highlight parathyroid and thyroid glands after simple intravenous injection, and to identify each gland simultaneously using the dual-NIR channel capability of the FLARE™ imaging system, suggests that head and neck surgery may someday be performed with increased precision and lower morbidity.

METHODS

Synthesis of T700 and T800 NIR fluorophores

All chemicals and solvents were of American Chemical Society grade or HPLC purity. Sigma-Aldrich (Saint Louis, MO) is the commercial source for the starting materials utilized in the presented synthesis and the reagents were used without purification. All compounds were obtained in high purity as indicated by TLC analyses and high-resolution ^{1}H and ^{13}C nuclear magnetic resonance (NMR) spectra. Chemical purity was measured by using ultra-performance liquid chromatography (UPLC, Waters, Milford, MA, USA) combined with simultaneous evaporative light scatter detection (ELSD), absorbance (photodiode array), fluorescence and electrospray time-of-flight (ESI-TOF) mass spectrometry (MS). See Supplementary Information for detailed chemical syntheses and analyses.

Optical and physicochemical property analyses

All optical measurements were performed at 37 °C in 100% fetal bovine serum (FBS) buffered with 50 mM HEPES, pH 7.4. Absorbance and fluorescence emission spectra of the series of NIR fluorophores were measured using fiber optic HR2000 absorbance (200–1100 nm) and USB2000FL fluorescence (350–1000 nm) spectrometers (Ocean Optics, Dunedin, FL). NIR excitation was provided by 5 mW of 655 nm red laser pointer (Opcom Inc., Xiamen, China) and 8 mW of 765 nm NIR laser diode light source (Electro Optical Components, Santa Rosa, CA) coupled through a 300 μm core diameter, NA 0.22 fiber (Fiberguide Industries, Stirling, NJ). For fluorescence quantum yield (QY) measurements, oxazine 725 in ethylene glycol (QY = 19%)[21] and ICG in DMSO (QY = 13%)[22] were used as calibration standards, under conditions of matched absorbance at 655 and 765 nm. *In silico* calculations of the partition coefficient (logD at pH 7.4) and total polar surface area (TPSA) were calculated using Marvin and JChem calculator plugins (ChemAxon, Budapest, Hungary).

Animal models

Animals were housed in an AAALAC-certified facility and were studied under the supervision of Beth Israel Deaconess Medical Center's Institutional Animal Care and Use Committee (IACUC) in accordance with approved institutional protocols (#101-2011 for rodents and #046-2010 for pigs). Male CD-1 mice weighing ≈ 25 g and male Sprague-Dawley (SD) rats weighing ≈ 250 g (Charles River Laboratories, Wilmington, MA) were anesthetized with 100 mg kg^{-1} ketamine and 10 mg kg^{-1} xylazine intraperitoneally

(Webster Veterinary, Fort Devens, MA). Female Yorkshire pigs (E.M. Parsons and Sons, Hadley, MA) averaging 35 kg were induced with 4.4 mg kg^{-1} intramuscular Telazol™ (Fort Dodge Labs, Fort Dodge, IA), intubated, and maintained with 2% isoflurane (Baxter Healthcare Corp., Deerfield, IL). Following anesthesia, electrocardiogram, heart rate, pulse oximetry, and body temperature were monitored throughout surgery.

NIR fluorescence imaging system

The dual-NIR channel FLARE™ imaging system has been described in detail previously[23–25]. In this study, 4 mW/cm^2 of 670 nm excitation light and 11 mW/cm^2 of 760 nm excitation light were used with white light (400–650 nm) at 40,000 lx. Color and NIR fluorescence images were acquired simultaneously with custom software at rates up to 15 Hz over a 15 cm diameter field of view. In the color-NIR merged image, 700 nm fluorescence (T700-F) and 800 nm fluorescence (T800-F) were pseudo-colored red and green, respectively. The imaging system was positioned at a distance of 18 inches from the surgical field. For each experiment, camera exposure time and image normalization were held constant.

Clinical study and mini-FLARE imaging system

This study was approved by the Medical Ethics Committee of the Leiden University Medical Center and was performed in accordance with the ethical standards of the Helsinki Declaration of 1975. All patients gave informed consent and were anonymized. NIR fluorescence imaging of the neck region was performed using the mini-FLARE imaging system, which has been described previously[25,26]. Briefly, the mini-FLARE system is composed of 2 NIR fluorescence: Channel #1 (656–678 nm excitation; 689–725 nm emission; 1.08 mW/cm^2 fluence rate) and Channel # 2 (745–779 nm excitation; 800–848 nm emission; 7.70 mW/cm^2 fluence rate). Of note, the working distance is up to 13 in. away from the patient, with field-of-view adjustable from 4.7 in. to 2 in. by moving the device toward or away from the surgical field.

Quantitative analysis

At each time point, the fluorescence and background intensity of a region of interest (ROI) over each tissue was quantified using custom FLARE™ software. The signal-to-background ratio (SBR) was calculated as SBR = fluorescence/background, where background is the signal intensity of neighboring muscle obtained over the imaging period. All NIR fluorescence images for a particular fluorophore were normalized identically for all conditions of an experiment. At least three animals were analyzed at each time point. Results were presented as mean ± s.d. and curve fitting was performed using Prism version 4.0a software (GraphPad, San Diego, CA).

Histology and NIR fluorescence microscopy

Parathyroid and thyroid tissues from rats and pigs were preserved for hematoxylin and eosin (H&E) and NIR fluorescence microscopic assessment. Tissues extracted from the animals post-intraoperative imaging were placed in 2% paraformaldehyde in PBS for 30 min before mounting in Tissue-Tek OCT compound (Fisher Scientific, Pittsburgh, PA) and flash-

freezing in liquid nitrogen. Frozen samples were cryosectioned (50 μm per slice), observed by fluorescence microscopy, then stained with H&E.

NIR fluorescence microscopy for resected tissues was performed on a 4 filter set Nikon Eclipse TE300 microscope system as previously described[27,28]. The microscope was equipped with a 100 W mercury light source (Chiu Technical Corporation, Kings Park, NY), NIR-compatible optics, and a NIR-compatible 10X Plan Fluor objective lens and a 100X Plan Apo oil immersion objective lens (Nikon, Melville, NY). Images were acquired on an Orca-AG (Hamamatsu, Bridgewater, NJ). Image acquisition and analysis was performed using iVision software (BioVision Technologies, Exton, PA). Two custom filter sets (Chroma Technology Corporation, Brattleboro, VT) composed of 650 ± 22 nm and 750 ± 25 nm excitation filters, 675 nm and 785 nm dichroic mirrors, and 710 ± 25 nm and 810 ± 20 nm emission filters were respectively used to detect T700-F and T800-F signals in the frozen tissue samples.

Supplementary Material

Refer to Web version on PubMed Central for supplementary material.

Acknowledgments

We thank David Burrington, Jr. for editing and Eugenia Trabucchi for administrative assistance. This study was supported by the following grants from the National Institutes of Health: NCI BRP grant #R01-CA-115296, NIBIB grant #R01-EB-010022 and #R01-EB-011523, and a grant from the Dana Foundation in Brain and Immuno-Imaging.

REFERENCES AND NOTES

1. Lee JH, Park G, Hong GH, Choi J, Choi HS. Design considerations for targeted optical contrast agents. Quant Imaging Med Surg. 2012; 2:266–273. [PubMed: 23289086]
2. Kobayashi H, Ogawa M, Alford R, Choyke PL, Urano Y. New strategies for fluorescent probe design in medical diagnostic imaging. Chem Rev. 2010; 110:2620–2640. [PubMed: 20000749]
3. Achilefu S. The insatiable quest for near-infrared fluorescent probes for molecular imaging. Angew Chem Int Ed Engl. 2010; 49:9816–9818. [PubMed: 21089086]
4. Pogue BW, Leblond F, Krishnaswamy V, Paulsen KD. Radiologic and near-infrared/optical spectroscopic imaging: where is the synergy? AJR Am J Roentgenol. 2010; 195:321–332. [PubMed: 20651186]
5. Gao J, et al. Ultrasmall near-infrared non-cadmium quantum dots for in vivo tumor imaging. Small. 2010; 6:256–261. [PubMed: 19911392]
6. Vahrmeijer AL, Hutteman M, van der Vorst JR, van de Velde CJ, Frangioni JV. Image-guided cancer surgery using near-infrared fluorescence. Nat Rev Clin Oncol. 2013; 10:507–518. [PubMed: 23881033]
7. Wang TS. Endocrine surgery. The American Journal of Surgery. 2011; 202:369–371. [PubMed: 21871991]
8. Lin DT, Patel SG, Shaha AR, Singh B, Shah JP. Incidence of inadvertent parathyroid removal during thyroidectomy. Laryngoscope. 2002; 112:608–611. [PubMed: 12150510]
9. Frilling, A.; Weber, F. Complications in thyroid and parathyroid surgery. Springer; New York: 2007.
10. Fancy T, Gallagher Dr, Hornig JD. Surgical anatomy of the thyroid and parathyroid glands. Otolaryngol Clin North Am. 2010; 43:221–227. vii. [PubMed: 20510710]

11. Bliss RD, Gauger PG, Delbridge LW. Surgeon's approach to the thyroid gland: surgical anatomy and the importance of technique. World J Surg. 2000; 24:891–897. [PubMed: 10865032]
12. Soshin T, et al. A method for sampling and tissue preparation of the parathyroid glands in miniature pigs for toxicity studies. J Toxicol Sci. 2010; 35:235–238. [PubMed: 20371975]
13. Kittel B, et al. Revised guides for organ sampling and trimming in rats and mice-Part 2. Exp Toxic Pathol. 2004; 55:413–431.
14. Gibbs-Strauss SL, et al. Nerve-highlighting fluorescent contrast agents for image-guided surgery. Mol Imaging. 2011; 10:91–101. [PubMed: 21439254]
15. Gibbs SL, et al. Structure-activity relationship of nerve-highlighting fluorophores. PLoS One. 2013; 8:e73493. [PubMed: 24039960]
16. van der Vorst JR, et al. Intraoperative near-infrared fluorescence imaging of parathyroid adenomas using low-dose methylene blue. Head & Neck. 2014; 36:853–858. [PubMed: 23720199]
17. Pollack G, Pollack A, Delfiner J, Fernandez J. Parathyroid surgery and methylene blue: A review with guidelines for safe intraoperative use. Laryngoscope. 2009; 119:1941–1946. [PubMed: 19598213]
18. McWade MA, et al. A novel optical approach to intraoperative detection of parathyroid glands. Surgery. 2013; 154:1371–1377. discussion 1377. [PubMed: 24238054]
19. Paras C, Keller M, White L, Phay J, Mahadevan-Jansen A. Near-infrared autofluorescence for the detection of parathyroid glands. J Biomed Opt. 2011; 16:067012. [PubMed: 21721833]
20. Lim YT, et al. Selection of quantum dot wavelengths for biomedical assays and imaging. Molecular imaging. 2003; 2:50–64. [PubMed: 12926237]
21. Sens R, Drexhage KH. Fluorescence quantum yield of oxazine and carbazine laser dyes. J Luminesc. 1981; 24:709–712.
22. Benson C, Kues HA. Absorption and fluorescence properties of cyanine dyes. J Chem Eng Data. 1977; 22:379–383.
23. Troyan SL, et al. The FLARE™ intraoperative near-infrared fluorescence imaging system: a first-in-human clinical trial in breast cancer sentinel lymph node mapping. Ann Surg Oncol. 2009; 16:2943–2952. [PubMed: 19582506]
24. Ashitate Y, et al. Two-wavelength near-infrared fluorescence for the quantitation of drug antiplatelet effects in large animal model systems. J Vasc Surg. 2012; 56:171–180. [PubMed: 22503225]
25. Gioux S, Choi HS, Frangioni JV. Image-guided surgery using invisible near-infrared light: fundamentals of clinical translation. Molecular imaging. 2010; 9:237–255. [PubMed: 20868625]
26. Mieog JS, et al. Toward optimization of imaging system and lymphatic tracer for near-infrared fluorescent sentinel lymph node mapping in breast cancer. Annals of surgical oncology. 2011; 18:2483–2491. [PubMed: 21360250]
27. Choi HS, et al. Rapid translocation of nanoparticles from the lung airspaces to the body. Nat biotechnol. 2010; 28:1300–1303. [PubMed: 21057497]
28. Choi HS, et al. Targeted zwitterionic near-infrared fluorophores for improved optical imaging. Nat Biotechnol. 2013; 31:148–153. [PubMed: 23292608]

a

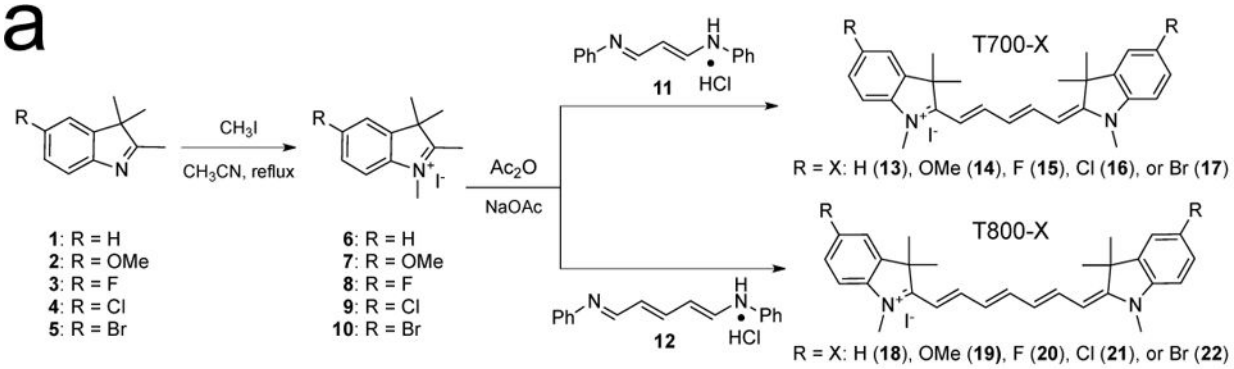

b

700 nm Fluorophores	**T700-H**	**T700-OMe**	**T700-F**	**T700-Cl**	**T700-Br**
Molecular Weight (Da)	383.55	443.60	419.53	452.44	541.34
LogD at pH 7.4	3.56	3.24	3.84	4.77	5.09
Total Polar Surface Area (Å^2)	6.25	24.71	6.25	6.25	6.25
Extinction Coefficient ($M^{-1}cm^{-1}$)	147,000	109,000	123,000	130,000	147,000
Absorbance Maximum (nm)	648	674	651	660	662
Emission Maximum (nm)	670	700	665	675	676
Stokes Shift (nm)	22	26	14	15	14
Quantum Yield (%)	30.4	10.4	29.9	27.6	27.0

800 nm Fluorophores	**T800-H**	**T800-OMe**	**T800-F**	**T800-Cl**	**T800-Br**
Molecular Weight (Da)	409.59	469.64	445.57	478.48	567.38
LogD at pH 7.4	4.08	3.77	4.37	5.29	5.62
Total Polar Surface Area (Å^2)	6.25	24.71	6.25	6.25	6.25
Extinction Coefficient ($M^{-1}cm^{-1}$)	115,000	98,000	110,000	148,000	150,000
Absorbance Maximum (nm)	758	785	758	770	774
Emission Maximum (nm)	770	804	771	785	790
Stokes Shift (nm)	12	19	13	15	16
Quantum Yield (%)	15.8	8.2	18.9	19.7	20.8

Figure 1.

(a) Synthetic schemes for T700 and T800 NIR fluorophores, and (b) their physicochemical and optical properties in 100% serum, pH 7.4. *In silico* calculations of logD at pH 7.4 and total polar surface area were calculated using Marvin and JChem calculator plugins (ChemAxon, Budapest, Hungary).

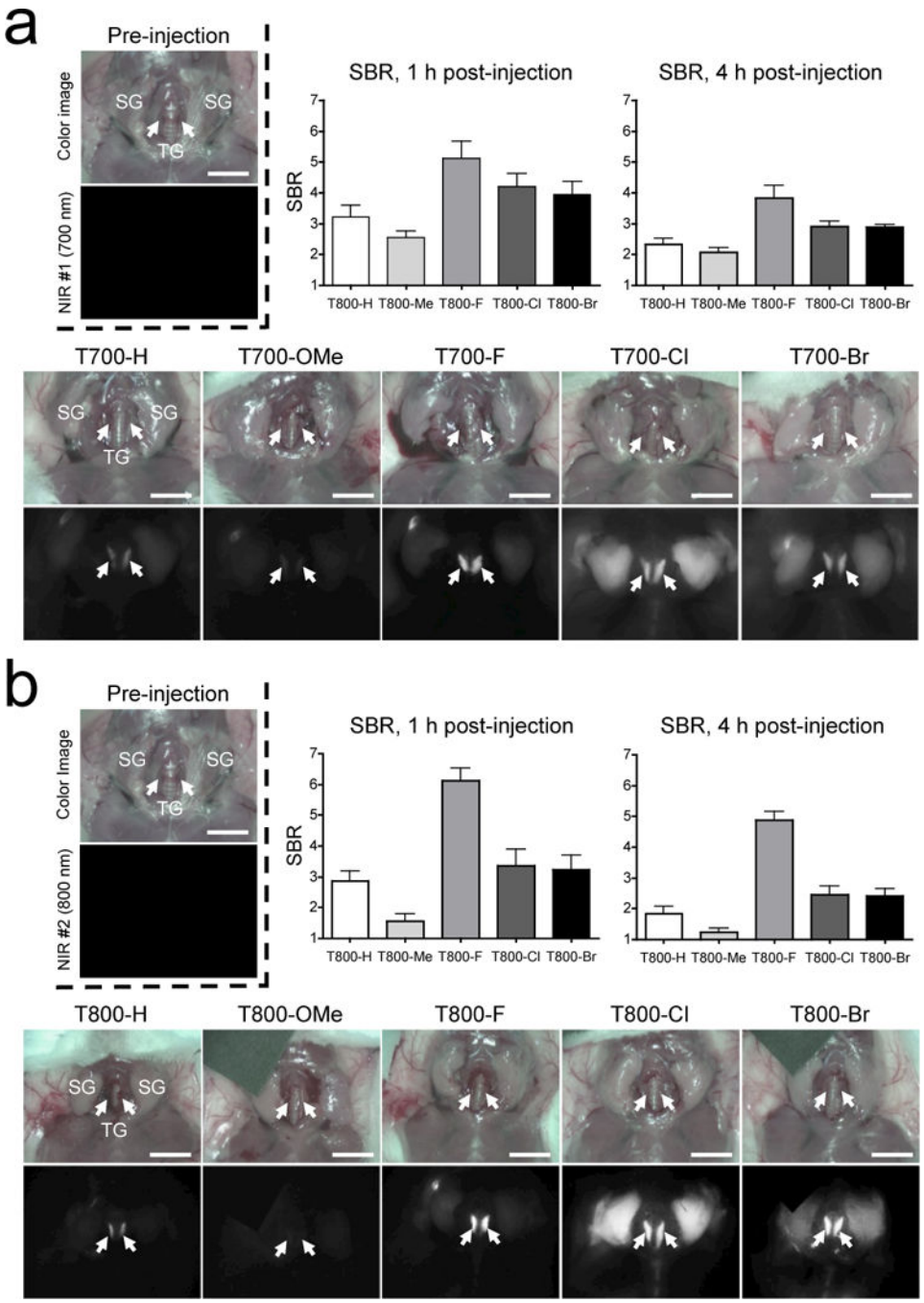

Figure 2.

In vivo thyroid targeting of (a) T700 and (b) T800 NIR fluorophores in mice. Each fluorophore was intravenously injected into 20 g CD-1 mice (10 nmol; 0.2 mg kg^{-1}) 1 h and 4 h prior to imaging. SBR was calculated by the fluorescence intensity of thyroid tissues versus the signal intensity of neighboring muscle obtained over the imaging period. All NIR fluorescence images have identical exposure and normalizations. Abbreviations used are: SG, salivary glands and TG, thyroid glands (arrows). Scale bars = 1 cm. Images are representative of n = 3 independent experiments at 1 h post-injection.

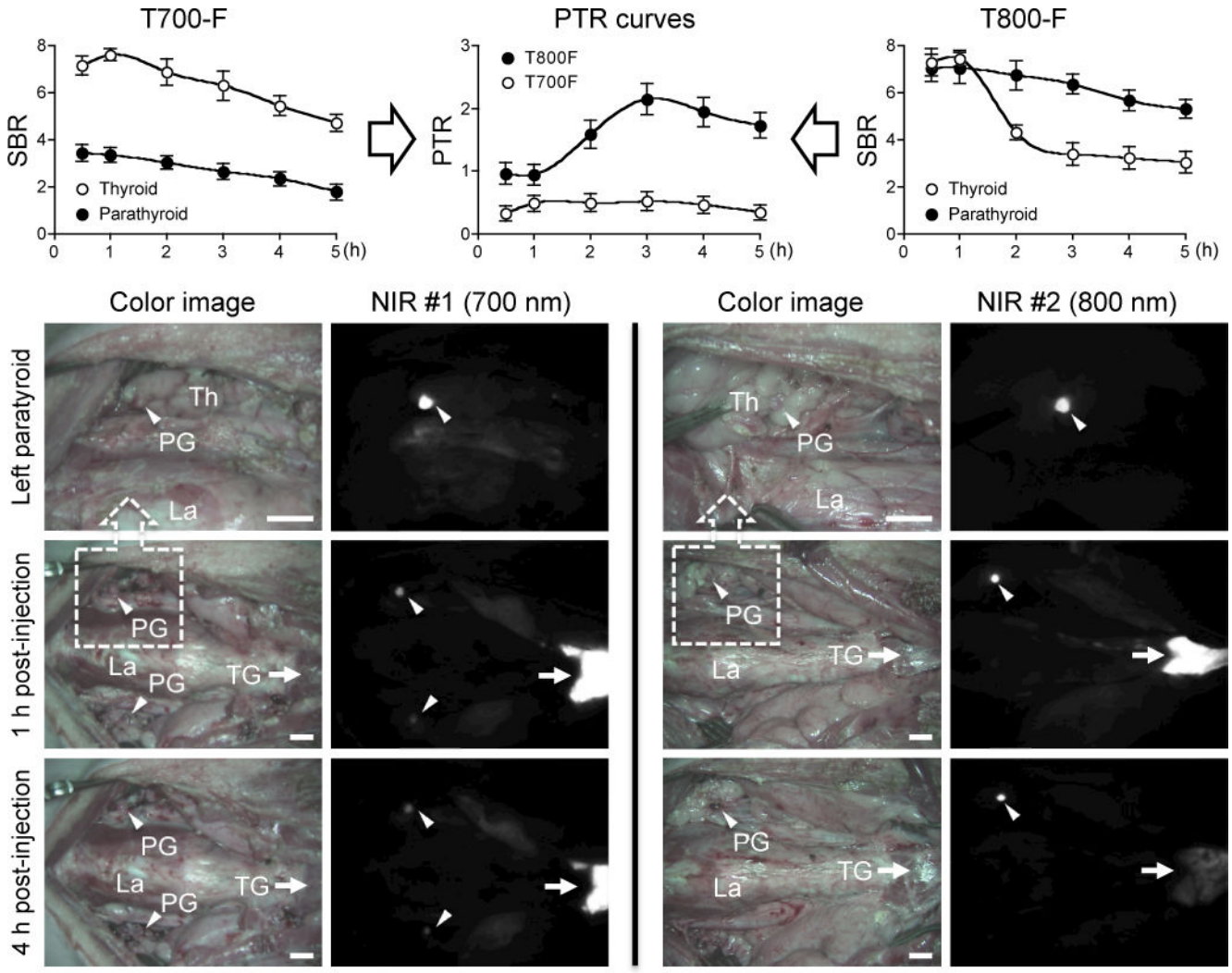

Figure 3.

In vivo parathyroid and thyroid imaging using T700-F and T800-F in pigs. 5 μmol (0.06 mg kg^{-1}) of T700-F and T800-F were injected intravenously into 35 kg Yorkshire pigs 5 h prior to imaging. All NIR fluorescence images have identical exposure and normalizations. SBR was calculated by the fluorescence intensity of each tissue versus the signal intensity of neighboring muscle obtained over the period of imaging time. Parathyroid signal to thyroid signal ratio (PTR) curves were determined from individual SBR curves. Abbreviations used are: La, larynx; PG, parathyroid glands (arrowheads); TG, thyroid gland (arrows), and Th, thymus. Scale bars = 1 cm. Each data point is the mean ± s.d. from n = 3 animals.

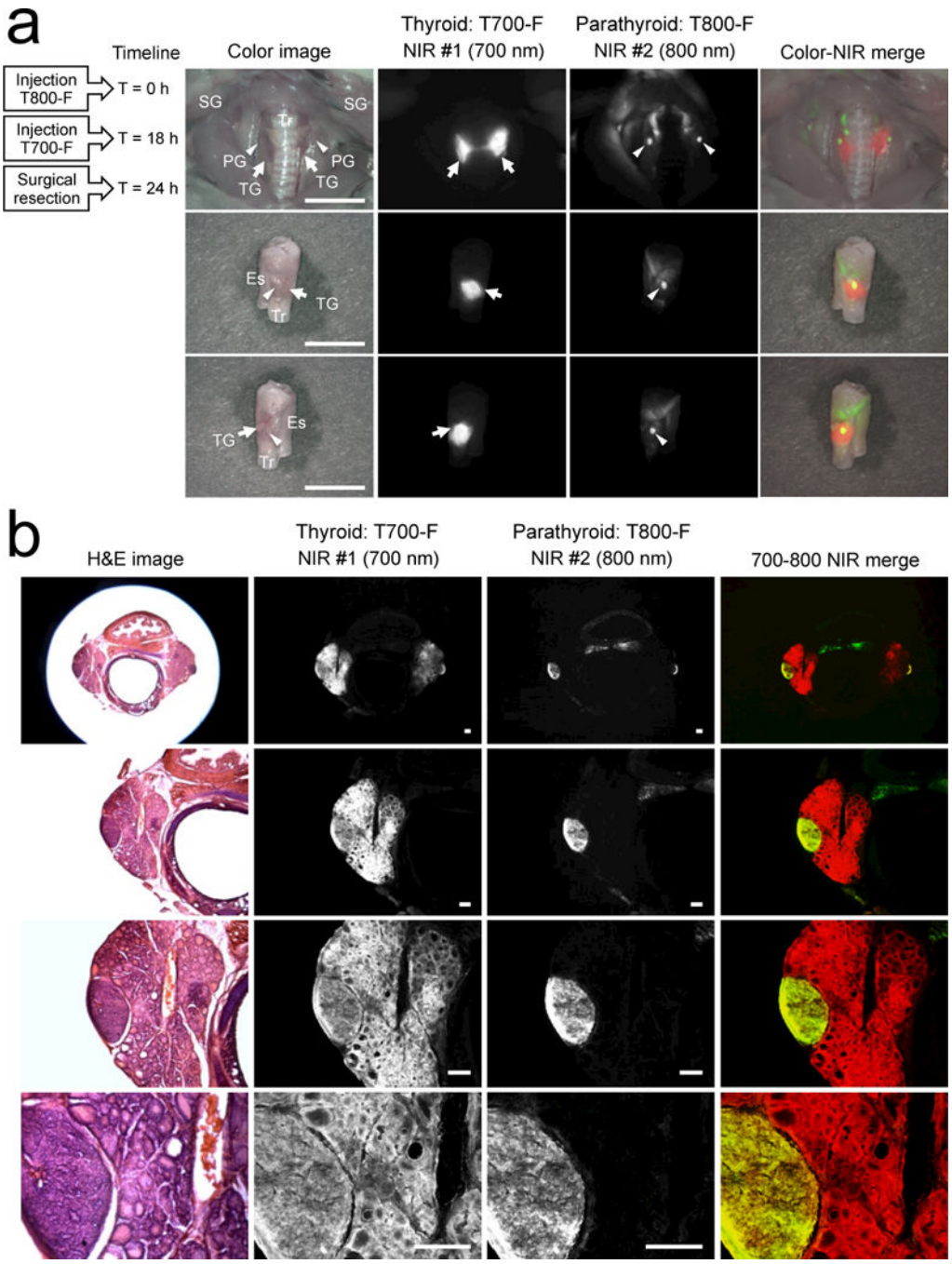

Figure 4.

(a) Dual-channel *in vivo* fluorescence imaging using T700-F and T800-F in the same rat. 0.2 μmol (0.35 mg kg^{-1}) of T800-F was intravenously injected into a 250 g SD rat 24 h prior to imaging, followed by 0.2 μmol of T700-F injected 6 h prior to imaging. Abbreviations used are: Es, esophagus; PG, parathyroid glands (arrowheads); SG, salivary glands; TG, thyroid glands (arrows); and Tr, trachea. Scale bars = 1 cm. (b) H&E and NIR imaging of resected parathyroid and thyroid tissues from (a). Scale bars = 300 μm. All NIR fluorescence images for each condition have identical exposure times and normalizations. Pseudo-colored red

and green colors were used for 700 nm and 800 nm channel images, respectively, in the color-NIR merged image.

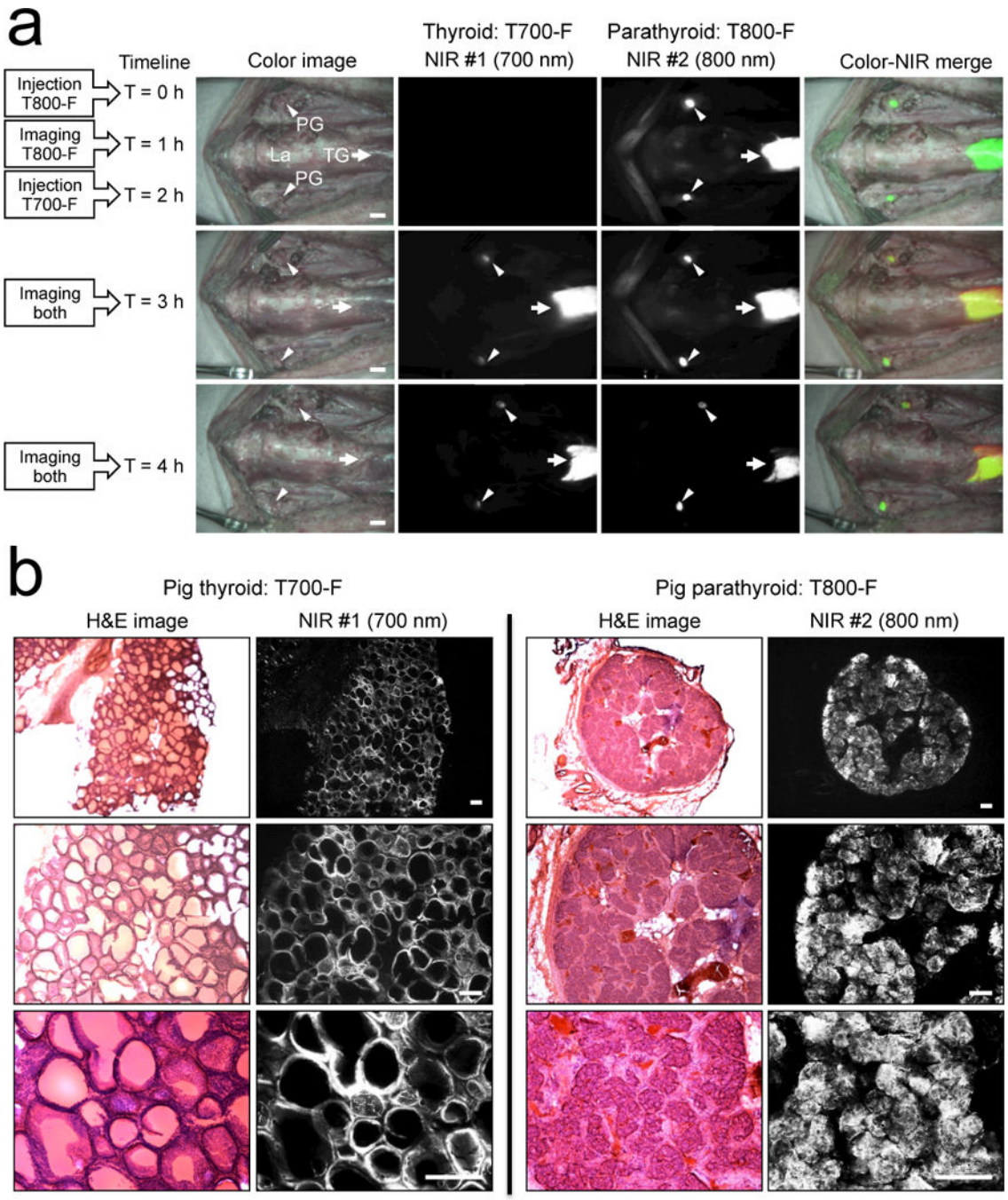

Figure 5.

(a) Dual-channel *in vivo* fluorescence imaging using T700-F and T800-F in the same pig. 5 μmol (0.06 mg kg^{-1}) of T800-F was intravenously injected into a 35 kg Yorkshire pig 4 h prior to imaging, followed by 5 μmol of T700-F injected 2 h later. Abbreviations used are: La, larynx; PG, parathyroid glands (arrowheads); and TG, thyroid gland (arrows). Scale bars = 1 cm. (b) H&E and NIR imaging of resected parathyroid and thyroid tissues from (a). Scale bars = 300 μm. All NIR fluorescence images have identical exposure and

normalizations. Pseudo-colored red and green colors were used for 700 nm and 800 nm channel images, respectively, in the color-NIR merged image.